Journal of Molecular Liquids 375 (2023) 121302

Contents lists available at ScienceDirect

Journal of Molecular Liquids

journal homepage: www.elsevier.com/locate/molliq

Structural evolution of the butylated hydroxytoluene/menthol hydrophobic eutectic solvent upon methanol and ethanol cosolvent addition

Giorgia Mannucci, Matteo Busato *, Alessandro Tofoni, Paola D'Angelo *

Department of Chemistry, University of Rome "La Sapienza", P.le A. Moro 5, Rome 00185, Italy

ARTICLE INFO

Article history:
Received 9 November 2022
Revised 10 January 2023
Accepted 19 January 2023
Available online 25 January 2023

Keywords:
Hydrophobic eutectic solvents
Menthol
Butylated hydroxytoluene
Ethanol
Methanol
Molecular dynamics
X-ray scattering

ABSTRACT

The changes upon methanol (MeOH) and ethanol (EtOH) addition in the structural arrangement of the hydrophobic eutectic solvent formed by butylated hydroxytoluene (BHT) and L-menthol (MEN) in 1:3 M ratio have been studied using molecular dynamics (MD) simulations integrated by small- and wide-angle X-ray scattering (SWAXS) measurements. Different mixtures containing the eutectic solvent and a variable amount of MeOH and EtOH have been investigated and the cosolvent introduction at any concentration has been found to break the hydrogen-bonds (H-bonds) among the MEN molecules, that are the most relevant interactions in the pristine eutectic, while the BHT component remains substantially non-interacting through all the explored composition range. This H-bond network is replaced by interactions between the MEN component and the cosolvent molecules, where the MEN species acts preferentially as H-bond donor towards the MeOH and EtOH molecules that behave mostly as H-bond acceptors. An increasing interplay between the excess cosolvent molecules is also observed upon increasing their concentration. SWAXS data show a contraction of the electron-dense regions corresponding to the hydroxyl groups upon cosolvent addition. This evidence is compatible with the intercalation of the MeOH and EtOH molecules in the MEN-MEN H-bond network to promote MEN-cosolvent and cosolvent-cosolvent interactions, in agreement with the MD results.

1. Introduction

Deep eutectic solvents (DESs) are mixtures of two or more compounds showing a melting point (MP) depression that is deeper than the ideally predicted one for at least one composition. This also implies that the MP of the eutectic is much lower than those of the individual parent compounds, allowing the achievement of a liquid phase even from solid starting materials. DESs often show interesting properties such as negligible volatility, high conductivity, non-flammability, high solvating capability, and low toxicity [1]. Furthermore, common DES components are biocompatible [2–4] and for these reasons they have been proposed as sustainable media targeting different applications such as extraction processes, energy storage, CO_2 capturing, catalysis, and drug delivery, among others [5,6]. DESs are also often indicated as "designing" solvents, meaning that their chemical-physical properties can be tuned to meet specific requirements through a judicious choice of the precursors and of their relative composition [1,7–9]. Recently, a new class of DESs composed solely of non-ionic compounds has been introduced: the so-called "type V" DESs [10]. This class includes hydrophobic deep eutectic solvents (HDESs), which were described for the first time in 2015 and have since then become the subject of numerous investigations [11–14]. The low water solubility of their components, often based on terpenes such as thymol and menthol, guarantees the formation of two phases at room temperature when put in contact with hydrophilic media, making these solvents ideal candidates for the setting-up of liquid–liquid biphasic extractions. For these reasons, they have been widely studied for the separation of target compounds like pesticides, [15] biomolecules,[11] medicinal components,[16] volatile fatty acids,[12] synthetic pigments,[17] and metal species [18–23].

Recently, a new hydrophobic eutectic with interesting properties has been presented, namely that formed by butylated hydroxytoluene (BHT) and L-menthol (MEN) [24,15,25–27,10]. The peculiarity of this mixture originates from the molecular structure of the BHT component, carrying a hydroxyl group that seems to be dramatically impeded in the formation of hydrogen-bonds (H-bonds) due to the presence of two *tert*-butyl groups in *ortho*

* Corresponding authors.
E-mail addresses: matteo.busato@uniroma1.it (M. Busato), p.dangelo@uniroma1.it (P. D'Angelo).

https://doi.org/10.1016/j.molliq.2023.121302
0167-7322/

positions (Fig. 1). This is in contrast with the mostly accepted view of eutectics and in particular of DESs, since the MP depression is often attributed to the extensive formation of a H-bond network between the components that act both as H-bond donors and acceptors [5,6,14]. Previous studies have demonstrated that a eutectic with a MP close to ideality can be obtained when the BHT and MEN compounds are mixed in a 1:3 molar ratio, allowing the achievement of a stable liquid phase suitable for room temperature operative conditions [24,25,28,27]. Notably, the BHT:MEN 1:3 system has been recently employed for successful liquid–liquid microextraction of pesticides and fat-soluble micronutrients from food samples [15,24].

Here, we extend previous studies on the BHT:MEN 1:3 mixture by inspecting the changes in the structural arrangement of the pristine eutectic caused by the introduction of two cosolvents, namely methanol (MeOH) and ethanol (EtOH). Indeed, interest has recently been devoted to DES mixtures with cosolvents, as the introduction of molecular species such as water or organic solvents has been demonstrated to seriously alter many DES chemical-physical properties, representing a further designing strategy that is more easily accessible than chemical modification of the parent compounds [29–38]. In particular, EtOH is frequently used as dispersing agent in extraction processes and represents a cheap strategy to lower the usually high viscosity of these mixtures [15,24,39]. On the other hand, MeOH is the smallest alcohol but its hydroxyl group enables the formation of a three-dimensional H-bond network similar to that of bulk water. Given the poor solubility of water in the BHT:MEN 1:3 eutectic, even for low concentrations,[24,25] MeOH addition allowed us to study the effect induced on this system by the organic solvent that most shares its properties with water. In addition, from a structural point of view it is of great interest to inspect the perturbation induced on the BHT:MEN 1:3 eutectic by the introduction of low molecular weight species with high H-bond donor/acceptor capabilities such as MeOH and EtOH. To this purpose, here we study BHT:MEN:MeOH and BHT:MEN:EtOH mixtures at different 1:3:*M* and 1:3:*E* molar ratios with a combined approach integrating molecular dynamics (MD) simulations and small- and wide-angle X-ray scattering (SWAXS) spectroscopy. Note that SWAXS has been widely employed to study DESs showing a marked sensitivity on the intermediate-range structural arrangement of these systems, while MD simulations are a precious tool to gain an atomistic description of both the local interactions and the longer-range structure of these systems [6,40,29,30,41,32,42,43]. This combined approach allows one to obtain an all-round structural picture about the evolution of the BHT:MEN 1:3 eutectic upon cosolvent addition.

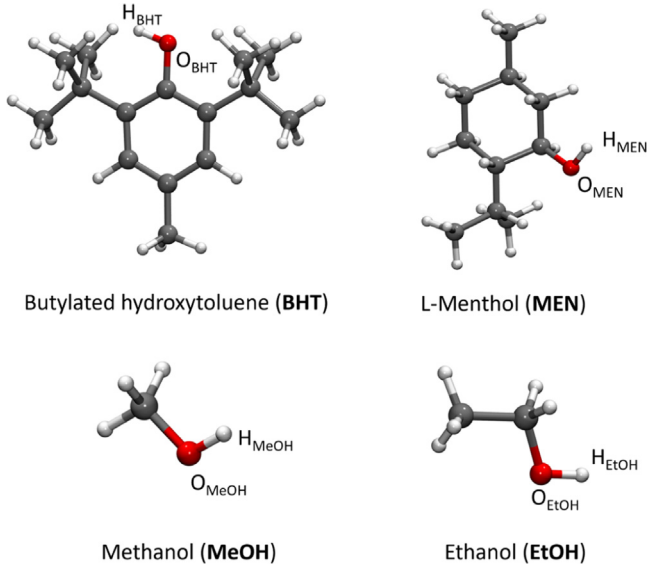

Fig. 1. Butylated hydroxytoluene (BHT), L-menthol (MEN), methanol (MeOH) and ethanol (EtOH) molecular structures showing the employed nomenclature for the studied atoms.

2. Materials and methods

2.1. Chemicals and sample preparation

BHT (food grade, $\geqslant 99\%$), MEN (natural source, food grade, $\geqslant 99\%$) and MeOH (99.8%) were purchased from Merck, while EtOH ($\geqslant 99.5\%$) was purchased from Carlo Erba Reagents S.r.l. The BHT:MEN 1:3 mixture was prepared by mixing the components at the desired molar ratio and then heating at 323 K until a colorless and viscous liquid was obtained. This eutectic solvent was used to prepare BHT:MEN:MeOH and BHT:MEN:EtOH mixtures at 1:3:*M* and 1:3:*E* molar ratios suitable for the SWAXS measurements, with *M* and *E* comprised between 1 and 26.

2.2. MD simulation details

Classical MD simulations have been carried out on the BHT:MEN:MeOH and BHT:MEN:EtOH mixtures at different 1:3:*M* and 1:3:*E* molar ratios using the Gromacs 2020.6 program [44]. Initial configurations were built by randomizing the atomic positions in cubic boxes (~50 Å side length) with the PACKMOL package[45] and a number of species chosen in order to reproduce the density of each mixture. Details about the studied systems are reported in Tables S1 and S2. The structures and interactions of BHT, MeOH, and EtOH were described by the all-atom optimized potentials for liquid simulation (OPLS/AA) force field [46], while for MEN the OPLS-compatible parameters developed by Jasik et al. were employed [47]. A cutoff radius of 12 Å was chosen for all the non-bonded interactions, while long-range electrostatic forces were computed with the particle mesh Ewald method [48,49]. Cross-terms for the Lennard-Jones interactions were constructed with the Lorentz-Berthelot combining rules. After an energy minimization, the simulation boxes were equilibrated in the NVT ensemble by gradually bringing the system from 300 to 500 K, keeping it at high temperature for 10 ns and gradually cooling down to 300 K. Production runs for data collection were carried out in the NVT ensemble for 50 ns at 300 K, using the Nosé-Hoover thermostat with a relaxation constant of 0.5 ps to control the temperature. The equations of motion were integrated with the leap-frog algorithm with a time step of 1 fs and all the stretching interactions involving hydrogen atoms were constrained with the LINCS algorithm [50]. The VMD 1.9.3 software was used for trajectories visualization [51]. The structural properties of the mixtures have been characterized by calculating site-site radial distribution function $g(r)$'s. In the case of the O-O distributions among the oxygen atoms of the mixtures the average distances have been obtained by modelling the $g(r)$'s with Gamma-like functions due to large the asymmetrys observed. This function depends on four parameters: the average distance *R*, the integration number *N*, the standard deviation σ^2, and the asymmetry index $\beta = 2p^{\frac{1}{2}}$. The general expression is:

$$g(r) = N\frac{p^{\frac{1}{2}}}{\sigma\Gamma(p)}\left(p + \frac{r-R}{\sigma}p^{\frac{1}{2}}\right)^{p-1} e^{-\left(p+\frac{r-R}{\sigma}p^{\frac{1}{2}}\right)} \quad (1)$$

where $\Gamma(p)$ is the Euler's Gamma function for the parameter *p*. This approach allows one to determine the average distance of the distribution that can be quite different from the maximum value in the case of highly asymmetric functions [52,53].

2.3. SWAXS measurements

SWAXS measurements were performed at the Austrian SAXS beamline of Elettra-Sincrotrone Trieste (Italy) by using an automatic sample changer system equipped with a Dectris Pilatus3 1 M detector [54]. Data were collected at room temperature on BHT:MEN:MeOH and BHT:MEN:EtOH mixtures at 1:3:*M* and 1:3:*E* molar ratios with *M* and *E* between 1 and 26. Calibration of the scattering vector q range, where $q = (4\pi sin\vartheta)/\lambda$, with 2ϑ being the scattering angle, was performed with a silver behenate standard. Measurements with different sample-detector distances were performed so that the overall explored q region was 0.05–1.8 $Å^{-1}$. The two-dimensional scattering patterns were subtracted for the dark counts, and then masked, azimuthally averaged, and normalized for transmitted beam intensity, exposure time, and subtended solid angle *per* pixel using the IGOR Pro software (IGOR Pro 7.0.8.1, Wavemetrics). The one-dimensional intensity *vs* q profiles was then subtracted for the empty capillary contribution and the different angular ranges were merged using the SAXSutilities2 tool [55].

3. Results and discussion

3.1. H-bond interactions: MD results

To obtain an atomistic description of the structural evolution of the BHT:MEN 1:3 eutectic upon MeOH and EtOH addition, MD simulations have been carried out on BHT:MEN:MeOH 1:3:*M* and BHT:MEN:EtOH 1:3:*E* mixtures for increasing *M* and *E* values (0 – 100). Pairwise radial distribution functions $g(r)$'s have been calculated for all the possible intermolecular H-O combinations involving the hydroxyl groups of the constituents, as this analysis can deliver key information about the extent of H-bond aggregation [29,30,41,32,43]. The employed nomenclature for the atom names is reported in Fig. 1. First, the description of the structural arrangement of the pristine BHT:MEN 1:3 eutectic is a mandatory starting point to quantify the perturbation induced by the cosolvents, which can be achieved by inspection of the H-O $g(r)$'s reported in Fig. 2 for *M* and *E* values equal to zero. Here, it can be observed that both the $H_{MEN} - O_{BHT}$ (Fig. 2a and 2b) and the $H_{BHT} - O_{BHT}$ (Fig. 2c and 2d) distributions show poorly structured peaks of negligible intensity, as the integration numbers *N* computed for a cutoff distance chosen at 3.45 Å resulted to be lower than 0.1 (Tables S3 and S4). Similarly, the $H_{BHT} - O_{MEN}$ $g(r)$ (Fig. 2e and 2f) shows a broad peak centered at about 3.00 Å, a distance that can hardly be associated with H-bonds [56]. On the other hand, the $H_{MEN} - O_{MEN}$ distribution shows a distinct peak centered at 2.01 Å (Figs. 2g and 2h), and integration of this curve up to a cutoff distance of 2.69 Å gives back a *N* value of 0.53. The whole result evokes a picture where the most relevant H-bonds established in the pristine BHT:MEN 1:3 eutectic are among MEN molecules, while those involving the BHT species acting either as H-bond donor or acceptor are negligible. This behavior is in agreement with previous findings attributing the low propensity of the BHT molecule to form H-bonds to the steric hindrance of the hydroxyl group due to the presence of the *tert*-butyl groups [24–26,10]. By looking at the evolution of the $g(r)$'s upon increasing *M* and *E* values it is possible to understand how the structural arrangement is perturbed by the introduction of the MeOH and EtOH cosolvents. Inspection of Fig. 2 reveals that the H-O distributions involving the BHT species remain almost identical in shape after cosolvent addition, and the observed decrease in intensity is due to the dilution of the eutectic (Figs. 2-a-2f). This behaviour is justified by the fact that the $g(r)$'s reported in Fig. 2 are multiplied by the numerical density of the observed atoms (ρ) to properly compare systems with different compositions, as already employed in previous works [29,30,41,43]. Still, the integration numbers obtained for these distributions remain close to zero throughout the entire explored composition range (see Tables S3 and S4). On the other hand, a decrease in intensity is observed also for the $H_{MEN} - O_{MEN}$ distribution, while the integration number for this interaction drops off through the series and reaches values close to zero for the highest cosolvent contents (Figure S1). Altogether these results show that addition to the BHT:MEN 1:3 eutectic of both MeOH and EtOH is not translated into an increase in the H-bond interactions that are already negligible in the pristine system, namely the BHT-MEN and BHT-BHT ones, while at the same time it is able to induce a serious perturbation in the MEN-MEN H-bond network.

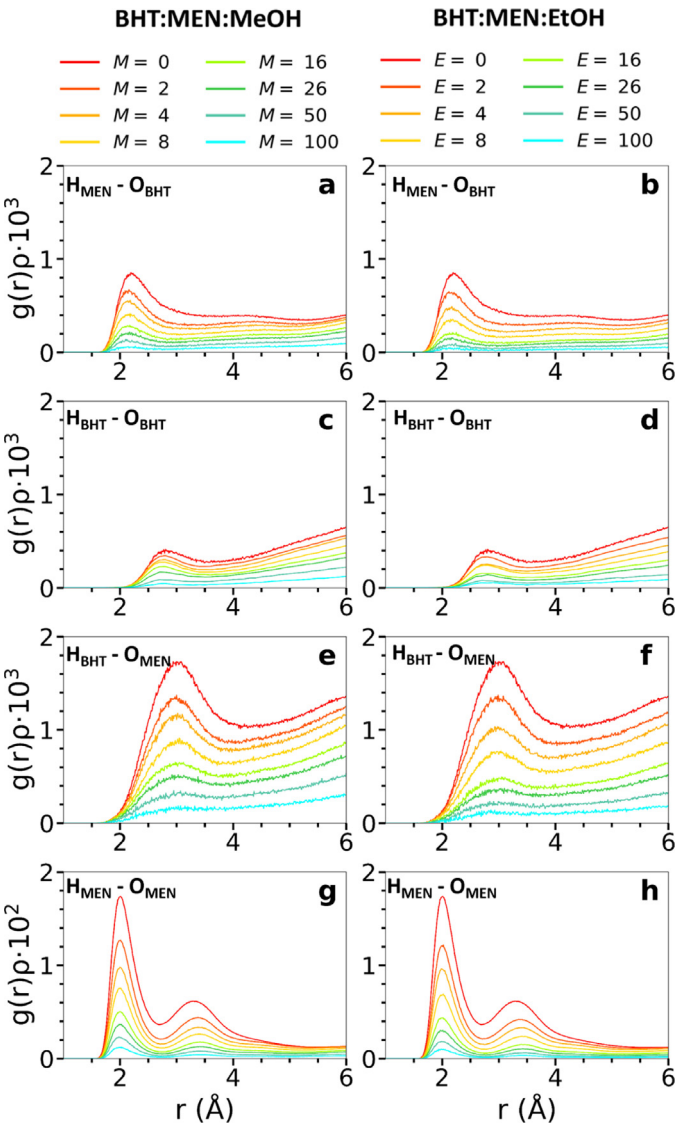

Fig. 2. Radial distribution functions multiplied by the numerical densities of the observed atoms, $g(r)\rho$'s, calculated from the MD simulations for the (a) $H_{MEN} - O_{BHT}$, (c) $H_{BHT} - O_{BHT}$ (e) $H_{BHT} - O_{MEN}$ and (g) $H_{MEN} - O_{MEN}$ pairs of the BHT:MEN:MeOH mixtures at different 1:3:*M* molar ratios and for the (b) $H_{MEN} - O_{BHT}$, (d) $H_{BHT} - O_{BHT}$, (f) $H_{BHT} - O_{MEN}$ and (h) $H_{MEN} - O_{MEN}$ pairs of the BHT:MEN:EtOH mixtures at different 1:3:*E* molar ratios.

Since addition of both MeOH and EtOH to the BHT:MEN 1:3 eutectic results in the disruption of the most relevant H-bonds present in the pristine system, the arising question is whether these interactions are somewhat replaced by other ones capable of preserving the overall H-bonds balance. To address this issue, we

inspected the behavior of the cosolvent through the explored composition range by means of the H-O $g(r)$'s involving the MeOH and EtOH molecules. As concerns the interaction with the BHT component, both the H_{BHT}-O_{MeOH} and H_{BHT}-O_{EtOH} distributions show no distinct peaks through all the series (Figures S2a and S2c). Similarly, the $H_{MeOH} - O_{BHT}$ and $H_{EtOH} - O_{BHT}$ $g(r)$'s show the presence of broad peaks integrating nearly zero even for high cosolvent concentrations (Figures S2b and S2d). The whole picture is indicative of the poor propensity of the BHT species to interact with the cosolvent molecules either in a H-bond donor or acceptor fashion. This is an interesting outcome since, although the steric hindrance of the hydroxyl group can reasonably be taken as the main factor that hampers the formation of H-bonds, one may think that small molecules with high H-bond donor/acceptor capabilities such as MeOH and EtOH could access the BHT hydroxyl site. Differently, these results show that this is not the case, giving a measure of how much the steric encumbrance provided by the two *tert*-butyl groups is detrimental for the establishment of H-bond interactions. Note that we also carried out preliminary MD simulations to study the behavior of water in the BHT:MEN 1:3 eutectic. In fact, although this system is hydrophobic, it can be supposed that a small amount of water molecules can be present in the eutectic when put in contact with an aqueous phase to form a biphasic system, like for example in a liquid–liquid biphasic extraction [15,24]. As a result, we obtained that the water molecule, which is the smallest species with H-bond donor/receptor capabilities, is not able to access the BHT hydroxyl group, giving a further confirmation of the hydrophobicity of the BHT component and ultimately of the BHT:MEN system.

Once the hypothesis that the introduced cosolvent may interact with the BHT species has been ruled out, we computed the H-O $g(r)$'s to inspect for possible MEN interactions with the MeOH and EtOH molecules (Figs. 3 and 4, respectively). All these distributions show distinct first peaks centered at about 2.00 Å and have a similar shape as that of the $H_{MEN} - O_{MEN}$ $g(r)$ of the pristine eutectic (Fig. 2g and 2h), which can be reasonably associated with H-bond interactions. However, while the $H_{MEN} - O_{MeOH}$ (Fig. 3a) and $H_{MEN} - O_{EtOH}$ (Fig. 4a) $g(r)$'s increase in intensity upon increasing cosolvent concentration, the opposite behavior is observed for the $H_{MeOH} - O_{MEN}$ (Fig. 3b) and $H_{EtOH} - O_{MEN}$ (Fig. 4b) ones. The same trend can be clearly observed from the evolution of the corresponding integration numbers of these curves as a function of the cosolvent content (Fig. 3d and Fig. 4d for MeOH and EtOH, respectively). The coordination numbers computed for a cutoff distance of 2.66 Åfor the BHT:MEN:MeOH 1:3:*M* system and of 2.75 Å for the BHT:MEN:EtOH 1:3:*E* one are reported in Tables S5 and S6. This result testifies a preferential H-bond donor behavior of the MEN species towards the introduced cosolvent, this being the main interaction replacing the MEN-MEN one present in the pristine eutectic. Note that this behavior is accompanied by an increase in the MeOH-MeOH and EtOH-EtOH H-bonds involving the excess of cosolvent molecules not interacting with the MEN species, as can be observed from the evolution of the $H_{MeOH} - O_{MeOH}$ (Fig. 3c) and $H_{EtOH} - O_{EtOH}$ (Fig. 4c) distributions and of the corresponding N values (Fig. 3d and Fig. 4d, respectively). Finally, it can be observed that the addition of both MeOH and EtOH perturbs the BHT:MEN 1:3 system in the same way, proving that slightly lengthening the alkyl chain of the cosolvent molecule does not lead to significant changes in the interactions between the latter and the eutectic components.

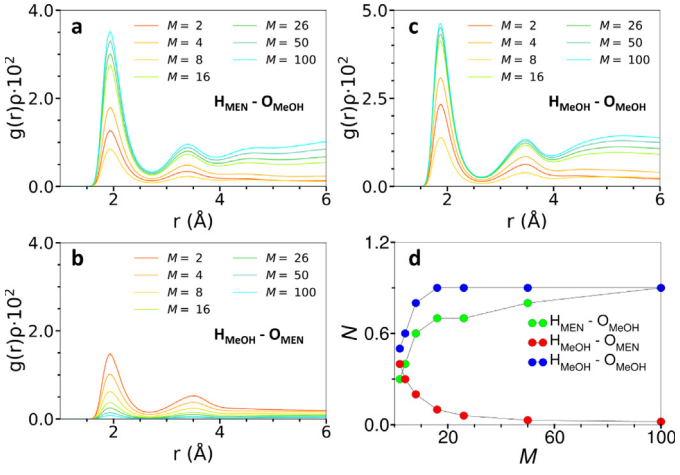

Fig. 3. Radial distribution functions multiplied by the numerical densities of the observed atoms, $g(r)\rho$'s, calculated from the MD simulations for the (a) $H_{MEN} - O_{MeOH}$, (b) $H_{MeOH} - O_{MEN}$, and (c) $H_{MeOH} - O_{MeOH}$ pairs from the MD simulations of the BHT:MEN:MeOH mixtures at different 1:3:*M* molar ratios. (d) Corresponding integration numbers *N*, calculated up to the first minimum of the $g(r)\rho$'s, plotted as a function of *M*.

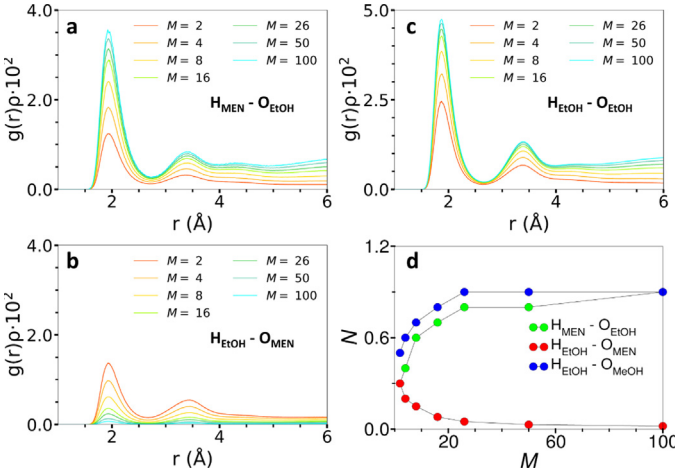

Fig. 4. Radial distribution functions multiplied by the numerical densities of the observed atoms, $g(r)\rho$'s, calculated from the MD simulations for the (a) $H_{MEN} - O_{EtOH}$, (b) $H_{EtOH} - O_{MEN}$, and (c) $H_{EtOH} - O_{EtOH}$ pairs from the MD simulations of the BHT:MEN:EtOH mixtures at different 1:3:*E* molar ratios. (d) Corresponding integration numbers *N*, calculated up to the first minimum of the $g(r)\rho$'s, plotted as a function of *E*.

3.2. Evolution of the intermediate-range structure

The effect of the presence of the cosolvent on the intermediate-range structural arrangement of the BHT:MEN 1:3 eutectic can be assessed from the SWAXS spectra collected on the BHT:MEN:MeOH and BHT:MEN:EtOH mixtures at different 1:3:*M* and 1:3:*E* molar ratios (Figs. 5a and 5b, respectively). At first glance, it can be observed that no spectral features are substantially present in the small-angle region (q <~0.5 Å^{-1}), that shows a flat profile for both the MeOH and EtOH mixtures. This is a non-trivial result, since the formation of nano-scale inhomogeneities in eutectic mixtures upon cosolvent addition has been previously detected by a marked increase in the small-angle scattered intensity [29,30]. Differently, the obtained WAXS profiles show at least two characteristic features able to deliver information about the intermediate-range aggregation in the studied mixtures. In particular, the WAXS main peak is preceded by a pre-peak at lower q values in all samples and this feature has been previously observed for menthol- and thymol-based eutectics and it has been associated to the steric exclusion between the carbon bodies of the constituents, preventing the formation of continuous H-bond networks. This structural

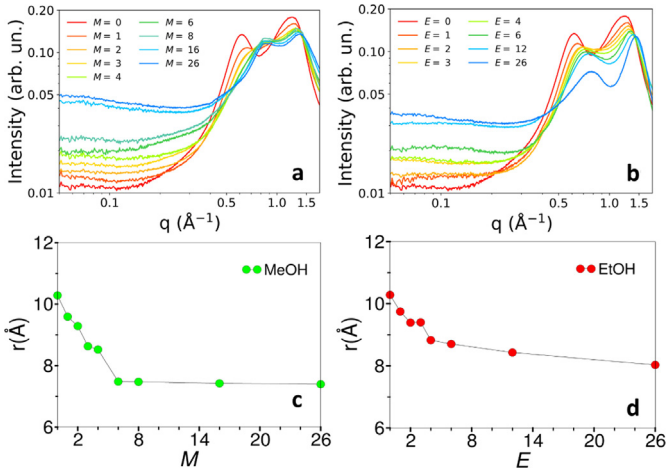

Fig. 5. Experimental SWAXS spectra collected on the (a) BHT:MEN:MeOH mixtures at different 1:3:*M* molar ratios and on the (b) BHT:MEN:EtOH mixtures at different 1:3:*E* molar ratios. Corresponding maximum position of the WAXS pre-peak in the direct space plotted as a function of (c) *M* and (d) *E*.

arrangement results in the intercalation between electron density-rich regions, corresponding to the H-bonded hydroxyl groups, interspersed by electron density-poor regions corresponding to the carbon bodies of the constituents [40,42,25]. In the case of the pristine BHT:MEN 1:3 eutectic, this pre-peak occurs at ∼0.63 Å^{-1} and corresponds to a distance of ∼10.3 Å in the real space, well compatible with the carbon-ring exclusion of the MEN and BHT components. However, this contribution is found to shift to higher *q* values as the cosolvent content increases, as can also be observed from the evolution of the peak positions in the real space reported as a function of the cosolvent molar ratio (Figs. 5c and 5d for MeOH and EtOH, respectively). The contraction of these electron-rich areas is compatible with the observed behavior of the introduced cosolvent molecules, which are able to perturb the MEN-MEN H-bond network and to promote both MEN-cosolvent and cosolvent-cosolvent interactions resulting in a shortening of the distances between the electron-denser oxygen atoms. This behavior can also be observed from a qualitative point of view from the MD snapshots taken on the entire simulations boxes reported in Fig. 6, where oxygen atoms contributing to the areas of higher electron density are shown as red surfaces, while carbon and hydrogen atoms are depicted in grey. Here, the shortening of the distances among the red areas upon increasing of both *M* and *E* values becomes evident. A more quantitative description of this behavior can be obtained from the $g(r)$'s computed between all the oxygen atoms for the BHT:MEN:MeOH 1:3:*M* and BHT:MEN:EtOH 1:3:*E* mixtures (Fig. 7a and b, respectively). As can be observed, quite asymmetric peaks are obtained with a maximum position clearly shortening to smaller distances upon increasing concentration. To better quantify this trend, these $g(r)$'s have been fitted with Gamma-functions to obtain the average distance of the O-O distribution, this one being different from the maximum distance because of the asymmetric shape of the $g(r)$. The obtained values are reported in Fig. 7c and 7d as a function of the *M* and *E* values, respectively. As a result, the shortening of the O-O distance upon increasing cosolvent concentration becomes evident, corroborating the experimental SWAXS evidence on the MD simulation results.

4. Conclusions

The structural changes induced by the addition of MeOH and EtOH cosolvents to the BHT:MEN 1:3 hydrophobic eutectic have been studied. MD simulations carried out on BHT:MEN:MeOH and BHT:MEN:EtOH mixtures at different 1:3:*M* and 1:3:*E* molar ratios show that the cosolvent addition provokes serious modifications to the structural arrangement of the pristine eutectic, where the most relevant H-bonds are between MEN molecules, while those involving the BHT component are negligible because of the high steric hindrance around its hydroxyl group. The MEN-MEN H-bond network is perturbed when MeOH and EtOH are added and these interactions are replaced by H-bonds between the MEN species and the cosolvent molecules. The MEN component shows a preferential H-bond donor behavior towards the cosolvent molecules, which in turn mostly act as H-bond acceptors. An increasing interplay among the excess cosolvent molecules is also observed upon increasing its concentration. Differently, the BHT molecule remains substantially non-interacting throughout all the explored composition range. SWAXS data show a contraction

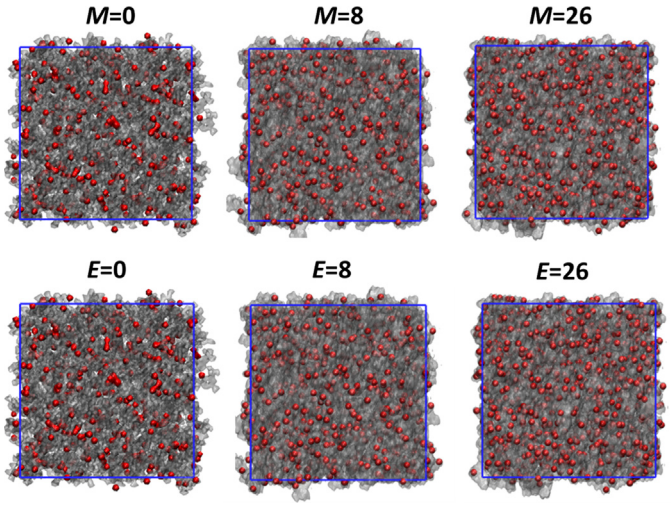

Fig. 6. Selected snapshots taken from the final configurations of the MD simulations performed on the BHT:MEN:MeOH mixtures at different 1:3:*M* molar ratios (top panels) and on the BHT:MEN:EtOH mixtures at different 1:3:*E* molar ratios (bottom panels). Oxygen atoms are shown in red, while carbon and hydrogen atoms in transparent grey. Box edges are highlighted by blue lines.

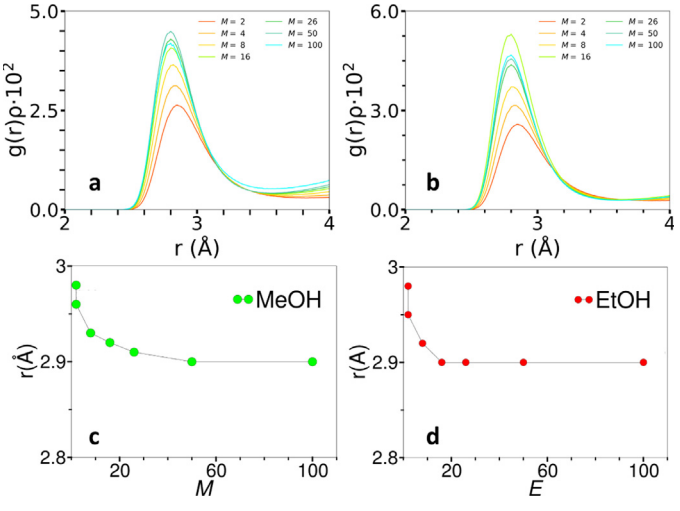

Fig. 7. Radial distribution functions multiplied by the numerical densities of the observed atoms, $g(r)\rho$'s, calculated for the O-O distribution among all the oxygen atoms from the MD simulations of the (a) BHT:MEN:MeOH mixtures at different 1:3:*M* molar ratios and of the (b) BHT:MEN:EtOH mixtures at different 1:3:*E* molar ratios. Corresponding average distance obtained after the fitting procedure with the Gamma-function plotted as a function of (c) *M* and (d) *E*.

of the distances among the electron-rich regions corresponding to the hydroxyl oxygen atoms through the series. This picture is compatible with the intercalation of the MeOH and EtOH molecules in the MEN-MEN H-bond network, promoting a progressive shortening of the hydroxyl group distances as a result of the increasing MEN-cosolvent and cosolvent-cosolvent interactions, in agreement with the MD results.

Declaration of Competing Interest

The authors declare that they have no known competing financial interests or personal relationships that could have appeared to influence the work reported in this paper.

Acknowledgements

Part of the calculations was performed on the Marconi100 system of the CINECA supercomputing center (grant IsC88-MDES2021). The authors acknowledge financial support from the Italian Ministry of University and Research (MIUR) through Grant PRIN 2017, 2017KKP5ZR, MOSCATo, and from the University of Rome "La Sapienza" Grant RG11916B702B43B9. The Austrian SAXS beamline of Elettra-Sincrotrone Trieste and its staff are acknowledged for synchrotron radiation beam time.

Appendix A. Supplementary material

Supplementary data associated with this article can be found, in the online version, at https://doi.org/10.1016/j.molliq.2023.121302.

References

[1] M. Francisco, A. van den Bruinhorst, M.C. Kroon, Angew. Chem. 52 (2013) 3074–3085.
[2] A. Paiva, R. Craveiro, I. Aroso, M. Martins, R.L. Reis, A.R.C. Duarte, A.C.S. Sustain, Chem. Eng. 2 (2014) 1063–1071.
[3] R. Craveiro, I. Aroso, V. Flammia, T. Carvalho, M. Viciosa, M. Dionísio, S. Barreiros, R. Reis, A. Duarte, A. Paiva, J. Mol. Liq. 215 (2016) 534–540.
[4] Y.H. Choi, J. van Spronsen, Y. Dai, M. Verberne, F. Hollmann, I.W. Arends, G.-J. Witkamp, R. Verpoorte, Plant Physiol. 156 (2011) 1701–1705.
[5] E.L. Smith, A.P. Abbott, K.S. Ryder, Chem. Rev. 114 (2014) 11060–11082.
[6] B.B. Hansen, S. Spittle, B. Chen, D. Poe, Y. Zhang, J.M. Klein, A. Horton, L. Adhikari, T. Zelovich, B.W. Doherty, B. Gurkan, E.J. Maginn, A. Ragauskas, M. Dadmun, T.A. Zawodzinski, G.A. Baker, M.E. Tuckerman, R.F. Savinell, J.R. Sangoro, Chem. Rev. 121 (2021) 1232–1285.
[7] S. Arnaboldi, A. Mezzetta, S. Grecchi, M. Longhi, E. Emanuele, S. Rizzo, F. Arduini, L. Micheli, L. Guazzelli, P.R. Mussini, Electrochim. Acta 380 (2021) 138189.
[8] M. Shi, W. Xiong, Z. Tu, X. Zhang, X. Hu, Y. Wu, Sep. Purif. Technol. 276 (2021) 119357.
[9] N. Zhang, Z. Huang, H. Zhang, J. Ma, B. Jiang, L. Zhang, Ind. Eng. Chem. Res. 58 (2019) 13321–13329.
[10] D.O. Abranches, M.A. Martins, L.P. Silva, N. Schaeffer, S.P. Pinho, J.A. Coutinho, Chem. Commun. 55 (2019) 10253–10256.
[11] B.D. Ribeiro, C. Florindo, L.C. Iff, M.A. Coelho, I.M. Marrucho, A.C.S. Sustain, Chem. Eng. 3 (2015) 2469–2477.
[12] D.J. Van Osch, L.F. Zubeir, A. van den Bruinhorst, M.A. Rocha, M.C. Kroon, Green Chem. 17 (2015) 4518–4521.
[13] D.J. Van Osch, C.H. Dietz, S.E. Warrag, M.C. Kroon, A.C.S. Sustain, Chem. Eng. 8 (2020) 10591–10612.
[14] D.O. Abranches, J.A. Coutinho, Curr. Opin. Green Sustain. Chem. 35 (2022) 100612.
[15] C. Dal Bosco, F. Mariani, A. Gentili, Molecules 27 (2022) 908.
[16] W. Tang, Y. Dai, K. Row, Anal. Bioanal. Chem. 410 (2018) 1–12.
[17] S. Zhu, J. Zhou, H. Jia, H. Zhang, Food Chem. 243 (2018) 351–356.
[18] Z. Yuan, H. Liu, W.F. Yong, Q. She, J. Esteban, Green Chem. 24 (2022) 1895–1929.
[19] N. Schaeffer, J.H.F. Conceição, M.A.R. Martins, M.C. Neves, G. Pérez-Sánchez, J.R. B. Gomes, N. Papaiconomou, J.A.P. Coutinho, Green Chem. 22 (2020) 2810–2820.
[20] G. Zante, M. Boltoeva, Sustain. Chem. 1 (2020) 238–255.
[21] N. Schaeffer, M.A.R. Martins, C.M.S.S. Neves, S.P. Pinho, J.A.P. Coutinho, Chem. Commun. 54 (2018) 8104–8107.
[22] D.J.G.P. Van Osch, D. Parmentier, C.H.J.T. Dietz, A. van den Bruinhorst, R. Tuinier, M.C. Kroon, Chem. Commun. 52 (2016) 11987–11990.
[23] E. Tereshatov, M.Y. Boltoeva, C. Folden, Green Chem. 18 (2016) 4616–4622.
[24] C. Dal Bosco, V. Di Lisio, P. D'Angelo, A. Gentili, A.C.S. Sustain, Chem. Eng. 9 (2021) 8170–8178.
[25] M. Busato, G. Mannucci, V. Di Lisio, A. Martinelli, A. Del Giudice, A. Tofoni, C. Dal Bosco, V. Migliorati, A. Gentili, P. D'Angelo, A.C.S. Sustain, Chem. Eng. 10 (2022) 6337–6345.
[26] M. Busato, G. Mannucci, V. Di Lisio, A. Martinelli, A. Del Giudice, A. Tofoni, C. Dal Bosco, V. Migliorati, A. Gentili, P. D'Angelo, A.C.S. Sustain, Chem. Eng. 10 (2022) 8671–8672.
[27] N. Schaeffer, L.P. Silva, J.A.P. Coutinho, A.C.S. Sustain, Chem. Eng. 10 (2022) 8669–8670.
[28] E. Burattini, P. D'Angelo, A. Di Cicco, A. Filipponi, N.V. Pavel, J. Phys. Chem. 97 (1993) 5486–5494.
[29] M. Busato, V. Di Lisio, A. Del Giudice, P. Tomai, V. Migliorati, L. Galantini, A. Gentili, A. Martinelli, P. D'Angelo, J. Mol. Liq. 331 (2021) 115747.
[30] M. Busato, A. Del Giudice, V. Di Lisio, P. Tomai, V. Migliorati, A. Gentili, A. Martinelli, P. D'Angelo, A.C.S. Sustain, Chem. Eng. 9 (2021) 12252–12261.
[31] O.S. Hammond, D.T. Bowron, K.J. Edler, Angew. Chem. Int. Ed. 56 (2017) 9782–9785.
[32] M. Busato, A. Tofoni, G. Mannucci, F. Tavani, A. Del Giudice, A. Colella, M. Giustini, P. D'Angelo, Inorg. Chem. 61 (2022) 8843–8853.
[33] Y. Dai, G.-J. Witkamp, R. Verpoorte, Y.H. Choi, Food Chem. 187 (2015) 14–19.
[34] Y. Wang, C. Ma, C. Liu, X. Lu, X. Feng, X. Ji, J. Chem. Eng. Data 65 (2020) 2446–2457.
[35] A.R. Harifi-Mood, R. Buchner, J. Mol. Liq. 225 (2017) 689–695.
[36] R. Alcalde, M. Atilhan, S. Aparicio, J. Mol. Liq. 272 (2018) 815–820.
[37] R. Haghbakhsh, S. Raeissi, J. Chem. Thermodyn. 124 (2018) 10–20.
[38] N.F. Gajardo-Parra, M.J. Lubben, J.M. Winnert, Ángel Leiva, J.F. Brennecke, R.I. Canales, J. Chem. Thermodyn. 133 (2019) 272–284.
[39] P. Tomai, A. Lippiello, P. D'Angelo, I. Persson, A. Martinelli, V. Di Lisio, R. Curini, C. Fanali, A. Gentili, Journal Chromatogr. A 1605 (2019) 360329.
[40] A. Malik, H.K. Kashyap, Phys. Chem. Chem. Phys. 23 (2021) 3915–3924.
[41] M. Busato, V. Migliorati, A. Del Giudice, V. Di Lisio, P. Tomai, A. Gentili, P. D'Angelo, PCCP 23 (2021) 11746–11754.
[42] N. Schaeffer, D.O. Abranches, L.P. Silva, M.A. Martins, P.J. Carvalho, O. Russina, A. Triolo, L. Paccou, Y. Guinet, A. Hedoux, et al., ACS Sustain. Chem. Eng. 9 (2021) 2203–2211.
[43] V. Migliorati, F. Sessa, P. D'Angelo, Chem. Phys. Lett. X 2 (2019) 100001.
[44] M.J. Abraham, T. Murtola, R. Schulz, S. Páll, J.C. Smith, B. Hess, E. Lindahl, SoftwareX 1 (2015) 19–25.
[45] L. Martínez, R. Andrade, E. Birgin, J. Martínez, J. Comput. Chem 30 (2009) 2157–2164.
[46] W.L. Jorgensen, D.S. Maxwell, J. Tirado-Rives, J. Am. Chem. Soc. 118 (1996) 11225–11236.
[47] M. Jasik, B. Szefczyk, J. Mol. Model. 22 (2016) 1–9.
[48] T. Darden, D. York, L. Pedersen, J. Chem. Phys. 98 (1993) 10089–10092.
[49] U. Essmann, L. Perera, M.L. Berkowitz, T. Darden, H. Lee, L.G. Pedersen, J. Chem. Phys. 103 (1995) 8577–8593.
[50] B. Hess, H. Bekker, H.J. Berendsen, J.G. Fraaije, J. Comput. Chem. 18 (1997) 1463–1472.
[51] W. Humphrey, A. Dalke, K. Schulten, J. Mol. Graph. 14 (1996) 33–38.
[52] F. Sessa, V. Migliorati, A. Serva, A. Lapi, G. Aquilanti, G. Mancini, P. D'Angelo, Phys. Chem. Chem. Phys. 20 (2018) 2662–2675.
[53] M. Busato, A. Lapi, P. D'Angelo, A. Melchior, J. Phys. Chem. B 125 (2021) 6639–6648.
[54] R. Haider, B. Sartori, A. Radeticchio, M. Wolf, S. Dal Zilio, B. Marmiroli, H. Amenitsch, J. Appl. Crystallogr. 54 (2021) 132–141.
[55] M. Sztucki, T. Narayanan, J. Appl. Crystallogr. 40 (2007) s459–s462.
[56] D. Herschlag, M.M. Pinney, Biochem. 57 (2018) 3338–3352.